TOWARD UNDERSTANDING LARGE DEFLECTION BENDING OF 3D PRINTED NINJAFLEX®

LUCAS K. GALLUP, MOHAMED TRABIA, BRENDAN O'TOOLE & YOUSSEF FAHMY
Department of Mechanical Engineering, University of Nevada-Las Vegas, USA

ABSTRACT

NinjaFlex® is a thermoplastic polyurethane filament that is primarily used for 3D printing. Aside from its low cost and availability, this material is highly flexible, durable, and has a low coefficient of friction. While NinjaFlex® was introduced approximately two decades ago, a comprehensive understanding of the filament's mechanical behavior, especially in the context of the effect of 3D printing, is still lacking. The goal of this research is to gain a better understanding of the behavior of 3D printed NinjaFlex® specimens when subjected to bending loads that cause large deflection. A series of experiments were conducted to test the bending of 3D printed dog-bone specimens with different rectangular cross sections and lengths. A total of 81 specimens were tested. Test fixtures were specifically designed for this goal. Camera and image processing techniques were used to measure the deflection of the specimens. The results indicate that the experimental setup achieved its goals with specimens experiencing a maximum deflection of about 33% of the specimen length. Assessment of the experimental results showed that specimens of the same dimensions and printed under the same conditions exhibit similar deflection. Experimental data are compared to a modified form of the Euler-Bernoulli beam theory. The results of this research will lead to a better understanding of the behavior 3D-printed thermoplastic polyurethane when it undergoes large deformation in bending and to better design 3D printed components.

Keywords: NinjaFlex, polyurethane, nonlinear material, large deflection bending, 3D printing.

1 INTRODUCTION

Development of 3D printers and materials has had a major impact on engineering designs and capabilities. The thermoplastic polyurethane (TPU) NinjaFlex® has proved itself to be a highly useful printing material. It has high flexibility, high durability, and a low coefficient of friction. Relatively recent introduction of the TPU into a field mainly occupied and maintained by hobbyists means that the methodical collection and analysis of its bending behavior has not been completed. It was the goal of this paper to conduct experiments to collect the bending deflection of specimens printed with NinjaFlex® filament.

There have been earlier attempts to understand the mechanical behavior of NinjaFlex®. For example, Reppel and Weinberg [1] studied the stress strain relationship and the rupture behavior of the NinjaFlex® shell specimens under uniaxial tensile loading by varying the shell thickness of 3D printed samples. They found that Ogden material model fitted the stress strain curves of the specimens accurately. Similarly, Messimer et al. [2] studied dog-bone shaped 3D printed NinjaFlex® specimens under axial loading. The specimens had the same geometry but were printed in three different orientations. Infill density was also varied. The effects of these parameters on the stress-strain curve were considered. They found that print orientations parallel to the length of the specimens had similar stress-strain curve. It was noticed that in all cases the stress-strain curves had very small elastic regions followed by a large nonlinear portion indicating a hyperplastic behavior. It was also noticed that the ultimate strength depended on the infill density and printing orientation. Pitaru et al. [3] investigated six different filament polymer materials, including NinjaFlex®, to test their mechanical properties under axial loading when the raster angle was changed. They

WIT Transactions on Engineering Sciences, Vol 133, © 2021 WIT Press
www.witpress.com, ISSN 1743-3533 (on-line)
doi:10.2495/MC210061

found that varying raster angle of the infill of the test specimens between 0, 45, and 90 degrees had a negative effect on the mechanical properties of NinjaFlex® specimens.

While these researchers provided necessary insights into the behavior of 3D printed NinjaFlex® components, they only focused on axial loading. The aim of this work was to understand the behavior of NinjaFlex® 3D printed parts in bending. We are especially interested in characterizing large deflection of beams in bending.

The remainder of this article is organized as follows. The methodology section lays out the setup, experimentation, and processing procedures. Experimental results section describes how the specimens behaved under bending as well as a comparison with classical beam theory.

2 NOMENCLATURE

a	Distance between end of specimen and the location of the applied point load, or the load offset.
b	Width of the center section of the dog-bone specimen.
E	Young's Modulus
h	Height of the center section of the specimen.
I	Area moment of inertia of the center section of the dog-bone specimen
L	Nominal length of the center section of the dog-bone specimen.
P	Applied point load.
P_{max}	Maximum applied point load.
y_{max}	Maximum defection of the center part of the specimen.
α	Nondimensionalized applied load.

3 METHODOLOGY

To test the bending behavior of NinjaFlex®, dog-bone shaped specimens were designed. A rectangular cross-section with circular ends were 3D printed (Fig. 1(a)). The specimens were printed with a 100% infill density and the same printing orientation (Fig. 1(b)). The dimensions of the center cross-section of the specimen were varied to study the effect of the geometry on the performance of the specimens, which had one end completely fixed while loads were applied to the other end.

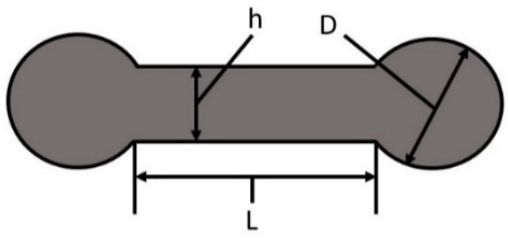

(a)

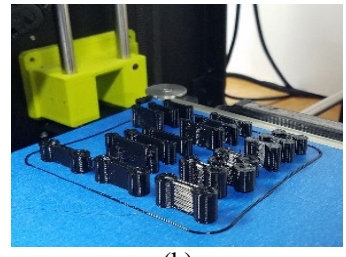

(b)

Figure 1: NinjaFlex® specimens. (a) Side view diagram; and (b) Printed specimens.

3.1 Test matrix

To understand the behavior of the material with respect to the physical dimensions, all three dimensions of the rectangular cross-section are varied between three values. Table 1 lists the values for the variable dimensions. The diameter of the cylindrical ends of the

specimens were dependent on the height of the cross section, *h,* as well as the distance from the point load to the end of the center of the specimen, *a*. Variables *h, b*, and *L* were varied between *S1*, *S2*, and *S3* for each value, resulting in a total of 27 different configurations of specimens. Three samples were printed for each size for a total of 81 different specimens. It should be noted that the length in Table 1 is nominal as the rectangular region of each specimen slightly overlaps with the clamped circular end sections of the specimen.

Table 1: Specimen test matrix; all values are in millimeters.

	S1	**S2**	**S3**
h	1.8	2.7	3.6
b	8	10	12
L (Nominal)	5	10	15
D	3.85	5.7	7.7
a	18.26	17.12	16.47

The NinjaFlex® specimens were printed using a LulzBot® Mini, manufactured by LulzBot®; all test specimens were printed in the same orientation with 100% infill density. Due to some filament stringing during the printing path, some anomalies were observed. These anomalies were physically removed if they were minor. Otherwise, specimens were reprinted. Once all parts were printed and ready, they were collected and stored in an organization box. The three test samples of each size were labeled with white paint on their sides as samples A, B, and C.

3.2 Test bracket

Test brackets were designed to hold either end of a specimen by inserting it through a recess. The bracket consists of two parts. The base bracket was used to attach the test specimen to a fixed support. The end bracket had an attachment hole near the end where a load was applied by hanging weights on a nylon fishing line. The brackets were printed on a Stratasys® Fortus 250mc, manufactured by Stratasys®, using ABSplus P430 material. The specimen ID, the load incrementation, number of loads, and maximum loads are listed in Table 2.

Fig. 2(a) shows the test bracket with a NinjaFlex® specimen inside a base bracket to the left, with a slotted groove for bolt attachment to an optical table. The right side of Fig. 2(a) shows the end bracket with the hole for attaching the point load. Fig. 2(b) shows an assembled specimen at no load. The photo shows a slight bend in the specimen due to the weight of the end bracket: 3.1, 2.9, and 2.7 grams for specimen height values 1.8, 2.7, and 3.6 mm respectively.

3.3 Experimental setup

Fig. 3 shows the experimental setup with labeled components. The trials were conducted on a worktable that contains a large grid of threaded anchor points. The test bracket, located on the left side of A, was bolted down with the test side hanging over the edge of the table. The test specimen, A, was put inside the bracket, and the other end of the specimen was put in the end piece bracket. A nylon fishing line with a knot on one end was inserted through the hole in the end bracket, to the right of label A. The other end of the fishing line was tied to a swivel hook for the weights, located between labels A and B.

Table 2: Specimen ID and loading parameters for all 27 specimen configurations.

ID	Minimum load (N)	Load increment (N)	Number of loads	Maximum load (N)
1	0.0304	0.0981	10	0.9133
2	0.0304	0.0981	11	1.0114
3	0.0304	0.0981	12	1.1095
4	0.0304	0.0491	11	0.5209
5	0.0304	0.0491	12	0.5700
6	0.0304	0.0491	13	0.6190
7	0.0304	0.0491	6	0.2757
8	0.0304	0.0491	8	0.3738
9	0.0304	0.0491	10	0.4719
10	0.0284	0.0981	17	1.5980
11	0.0284	0.0981	19	1.7942
12	0.0284	0.0981	21	1.9904
13	0.0284	0.0491	23	1.1075
14	0.0284	0.0491	27	1.3037
15	0.0284	0.0491	31	1.4999
16	0.0284	0.0491	15	0.7151
17	0.0284	0.0491	18	0.8623
18	0.0284	0.0981	11	1.0094
19	0.0265	0.1962	12	2.1847
20	0.0265	0.1962	13	2.3809
21	0.0265	0.1962	13	2.3809
22	0.0265	0.1962	11	1.9885
23	0.0265	0.1962	12	2.1847
24	0.0265	0.1962	14	2.5771
25	0.0265	0.0981	16	1.4980
26	0.0265	0.0981	21	1.9885
27	0.0265	0.0981	26	2.4790

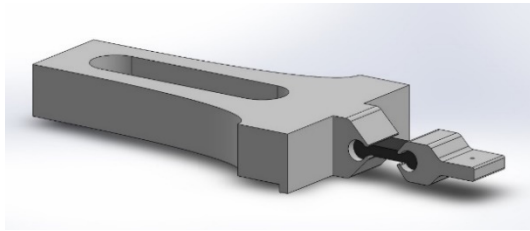

(a)

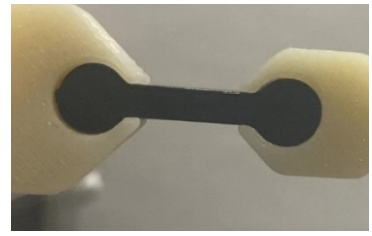

(b)

Figure 2: (a) Test bracket with NinjaFlex® specimen assembly; (b) Printed specimens.

A white board was placed behind the specimen to reduce unnecessary objects captured by the camera in the experiment. A camera was placed in the camera bracket in front of the brackets and specimen, B. A sheet metal was held above the setup with an articulating arm to reduce the glare on the top surface of the specimen cause by the ambient light in the lab.

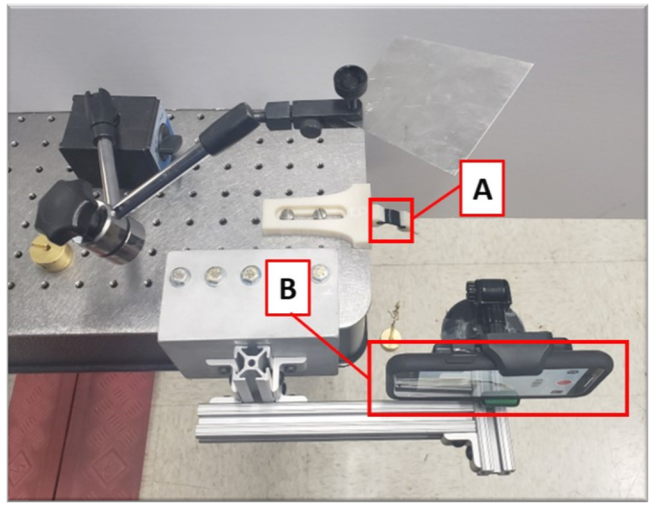

Figure 3: Labeled test setup. (A) is the test specimen and (B) is the camera.

3.4 Data collection

The data collected in the experiments were in the form of videos. The videos were captured using an iPhone 11 Pro® at 4k resolution and 60 fps. Matlab® Camera Calibration Toolbox was used to identify the intrinsic and extrinsic characteristics of the lens and thereby removing any potential distortion of the images. The camera calibration was conducted at the beginning of each experimental session.

Once calibration was completed, weights were attached to the end of the nylon line on the free end bracket in varying increments until a vertical deflection of approximately one third of the length of the center portion of the specimen was achieved. The maximum weight needed to reach this goal depended on the dimensions of the specimen.

3.5 Image processing

A custom Matlab® code was created to automatically process the images resulting from each experiment. This code used various functions of Matlab® Computer Vision Toolbox. Images were extracted from the experimental video corresponding to each load increment. Fig. 4(a) shows a typical example.

The images were undistorted based on the camera calibration results and converted to grayscale, Fig. 4(b). Next, the pixels of the images were cropped to emphasize the specimen and then converted to binary values using a custom algorithm, Fig. 5(a). The cylindrical ends of the specimen were identified using a built-in function from said Toolbox, Fig. 5(b). The radii of these circles were increased by ten pixels to account for the nonuniform contour of these circles due to pixilation. Pixels inside these two circles were converted to black, Fig. 5(c), leaving the center part of the specimen only in the images. The four edges of the remaining area were identified, Fig. 5(d). Two sets of equal number of points on the top and bottom edges were identified. Each pair of respective points were averaged to identify the corresponding point on the neutral axis, Fig. 5(e). Second-order polynomials were found to fit the top and bottom edges as well as the neutral axis, Fig. 5(f).

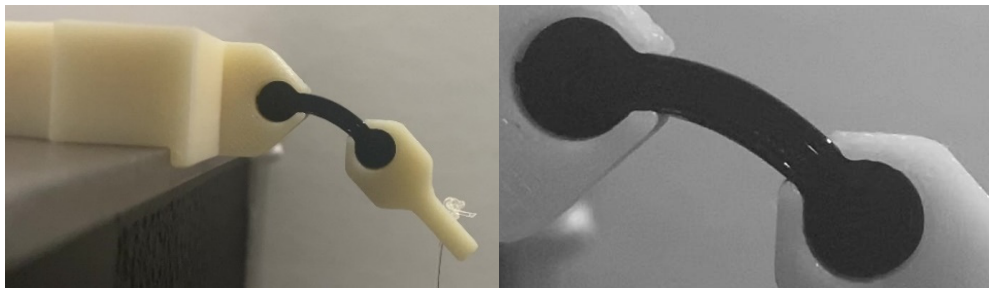

(a) (b)

Figure 4: (a) Raw image pulled from experiment video, specimen h = 2.7 mm, b = 8 mm, L = 10 mm nominal, Load 113 grams; and (b) Cropped and zoomed grayscale conversion of raw image.

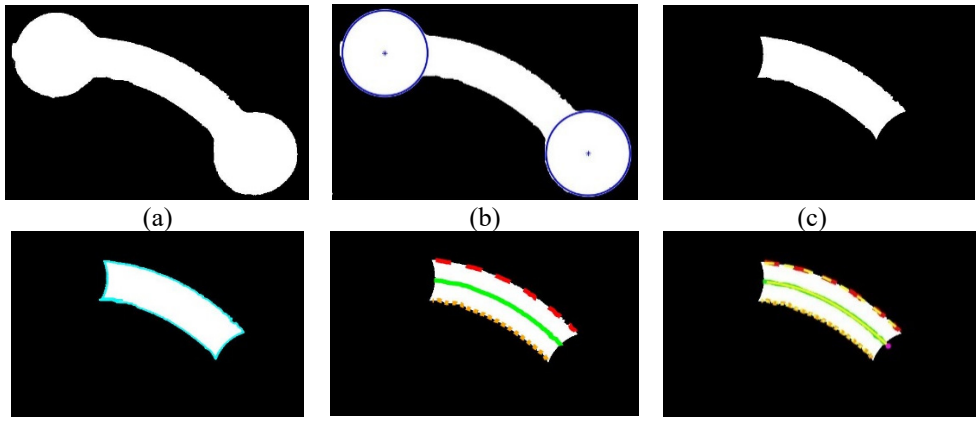

(a) (b) (c)

(d) (e) (f)

Figure 5: Stages of processing a specimen. (a) Cropped image converted to a binary image; (b) Detection of rounded ends of specimen; (c) Removal of rounded sections; (d) Boundary detection; (e) Top edge, bottom edge, and neutral axis detection; and (f) Curve fitting of top and bottom edges and neutral axis (yellow).

The point used to measure deflection was identified as the intersection of the neutral axis fitted curve and the edge of the free end cylindrical section that was identified earlier, Fig. 6. The deflection of the three samples with identical geometry were averaged, and the corresponding standard deviation was determined.

4 EXPERIMENTAL RESULTS

Table 3 summarizes the specimen geometry and results of these experiments. The resulting bending of the specimens followed the general expected behavior of a bending beam. To help clarify the results, Fig. 7 shows the deflection of beams with the same cross-sectional area and varying lengths. Reported results are the averages of the three samples. The

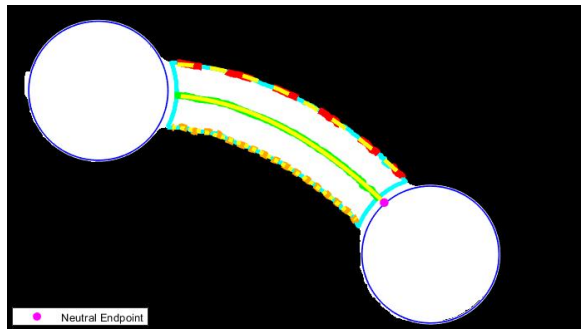

Figure 6: Final processed image, (113 grams).

increased angle at the point of load application means that the load component causing bending was gradually reduced while a load component that extends the beam was increasing. Due to the decrease in required load for desired deflection some specimens were tested with fewer loads, which can be seen in Fig. 7.

Table 3: Specimen geometry and experimental results.

ID	h (mm)	b (mm)	L (mm)	Maximum load (N)	Average x_{max}/L	Average y_{max}/L	Std. dev. x_{max}/L	Std. dev. $y_{max/L}$
1	1.8	8	6.925	0.9133	0.7724	0.3129	0.0171	0.0066
2	1.8	10	6.925	1.0114	0.6871	0.2803	0.0265	0.0041
3	1.8	12	6.925	1.1095	0.8870	0.2936	0.0619	0.0110
4	1.8	8	11.925	0.5209	0.7858	0.4296	0.0099	0.0207
5	1.8	10	11.925	0.5700	0.9327	0.4310	0.0058	0.0070
6	1.8	12	11.925	0.6190	0.8780	0.3827	0.1287	0.0538
7	1.8	8	16.925	0.2757	0.9145	0.4997	0.0039	0.0107
8	1.8	10	16.925	0.3738	0.8495	0.5366	0.0503	0.0021
9	1.8	12	16.925	0.4719	0.8532	0.4732	0.0158	0.0260
10	2.7	8	7.850	1.5980	0.9821	0.2480	0.0042	0.0062
11	2.7	10	7.850	1.7942	0.9726	0.2204	0.0108	0.0013
12	2.7	12	7.850	1.9904	1.0029	0.2126	0.0033	0.0044
13	2.7	8	12.850	1.1075	0.9506	0.3788	0.0097	0.0025
14	2.7	10	12.850	1.3037	0.9204	0.3433	0.0226	0.0068
15	2.7	12	12.850	1.4999	0.9398	0.3593	0.0016	0.0045
16	2.7	8	17.850	0.7151	0.8889	0.3585	0.0394	0.0211
17	2.7	10	17.850	0.8623	0.9198	0.3607	0.0062	0.0115
18	2.7	12	17.850	1.0094	0.9103	0.3598	0.0173	0.0120
19	3.6	8	8.850	2.1847	0.9594	0.2323	0.0085	0.0138
20	3.6	10	8.850	2.3809	0.8851	0.1875	0.0101	0.0067
21	3.6	12	8.850	2.3809	0.9458	0.1857	0.0037	0.0213
22	3.6	8	13.850	1.9885	0.8534	0.3853	0.0188	0.0189
23	3.6	10	13.850	2.1847	0.9448	0.3245	0.0199	0.0045
24	3.6	12	13.850	2.5771	0.9004	0.3149	0.0347	0.0015
25	3.6	8	18.850	1.4980	0.9251	0.4290	0.0188	0.0300
26	3.6	10	18.850	1.9885	0.8957	0.4554	0.0044	0.0127
27	3.6	12	18.850	2.4790	0.8801	0.4065	0.0306	0.0057

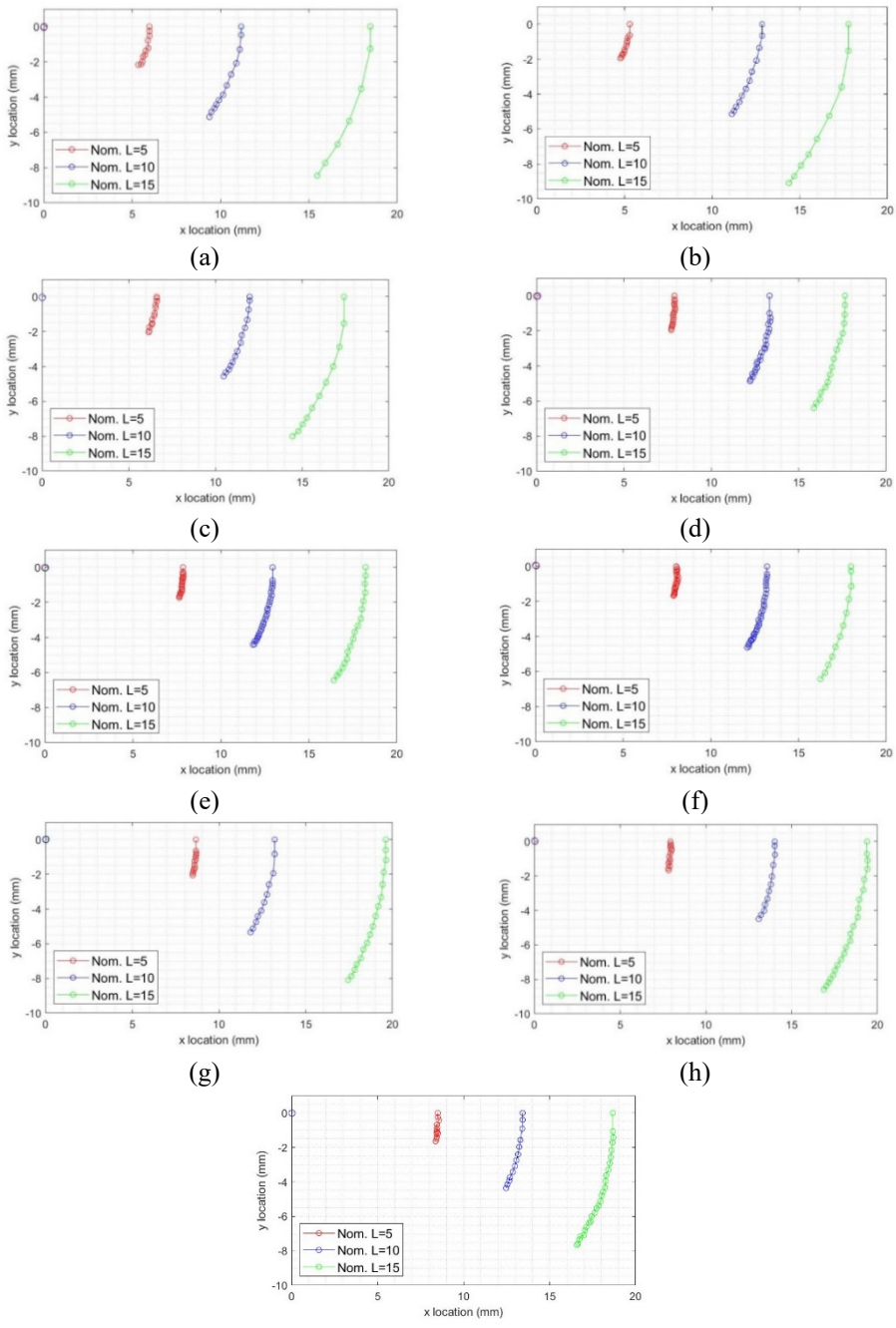

Figure 7: Deflection of specimens with the same cross-sectional area, height by width. (a) 1.8 mm by 8 mm; (b) 1.8 mm by 10 mm; (c) 1.8 mm by 12 mm; (d) 2.7 mm by 8 mm; (e) 2.7 mm by 10 mm; (f) 2.7 mm by 12 mm; (g) 3.6 mm by 8 mm; (h) 3.6 mm by 10 mm; and (i) 3.6 mm by 12 mm.

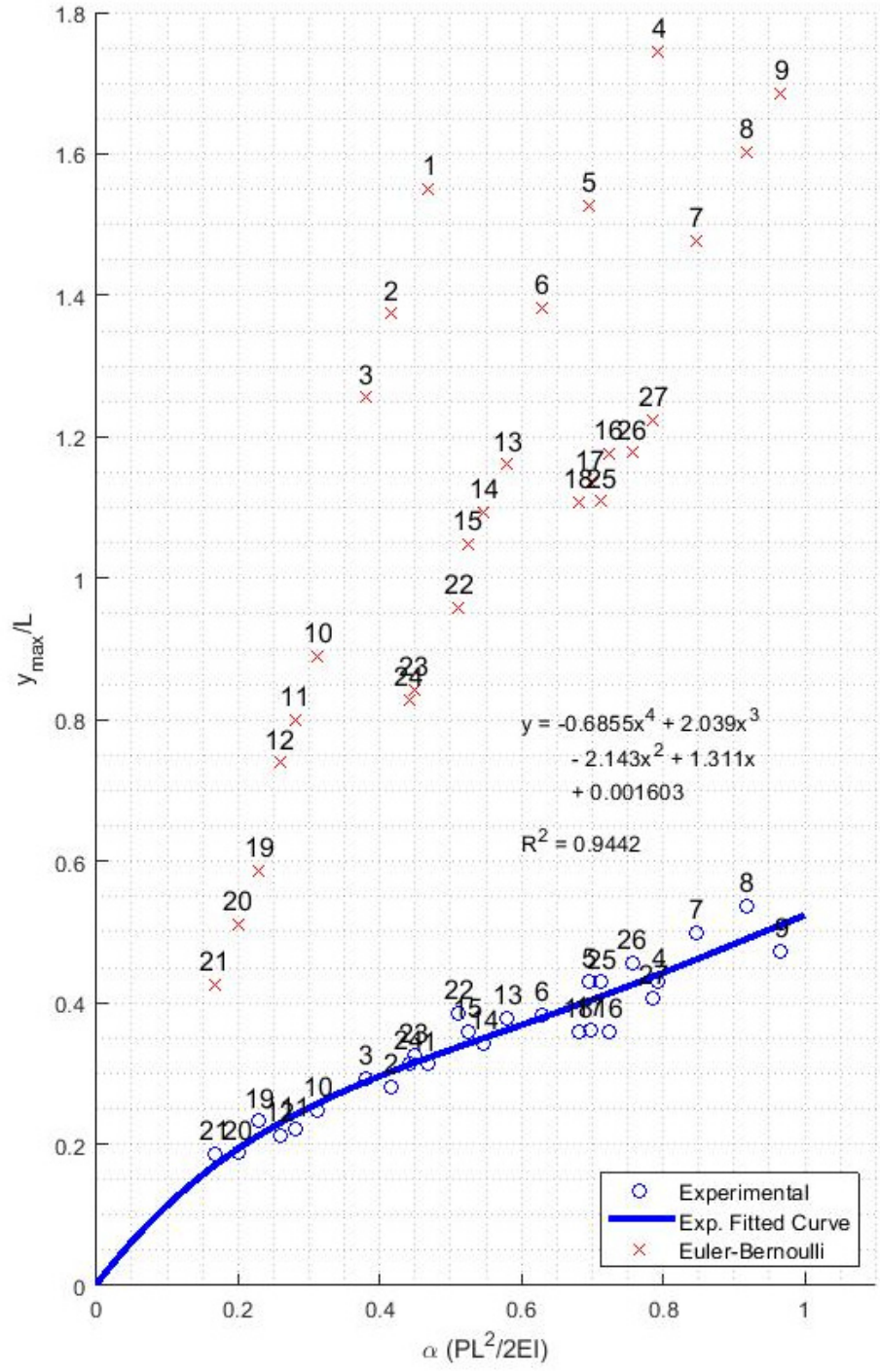

Figure 8: Non-dimensional analysis of specimen performance with modified theoretical Euler-Bernoulli equations and fitted curve with equation.

The maximum deflections in the vertical and horizontal directions were nondimensionalized by dividing each of them by the specimen nominal length, L. The maximum applied force was nondimensionalized using a variable, α:

$$\alpha = \frac{P_{max}L^2}{2EI}. \quad (1)$$

Since the NinjaFlex® material can bend approximately 35% vertically with respect to the length and the load arm of the force changes with respect to the beam's slope at the endpoint, a modified version of Euler-Bernoulli will be used to approximate the bending of the specimen. It differs from the traditional theory by including deflection for both the point and moment load, eqns (2) and (3) respectively. Using superposition, a theoretical value for y_{max} was calculated by adding these two terms:

$$y_{max} = \frac{P_{\max}(L+a)^3}{3EI} + \frac{P_{\max}aL^2}{2EI}. \quad (2)$$

Fig. 8 shows the nondimensionalized maximum vertical deflection, y_{max}/L, plotted against α, the nondimensionalized applied maximum load from eqn (1). The experimental material behavior followed an approximate fourth-order polynomial trend. The R^2 value for the fitted curve was 0.9442. The red markers denote a theoretical response that should have been expected based on the modified equations. The theoretical predictions show a linear function of applied load and do not account for the nonlinear large deflections of the NinjaFlex® material. The labeled points and their corresponding dimensions can be found in Table 2.

There were several major trends in the plot. Firstly, specimens that had the same nominal length with varied depths were found grouped close together in Fig. 8, i.e., groups of three. Within these groups there was a general trend for the specimens with a larger depth to have a lower value in both the x and y axis. Similarly, specimens with the same depth and nominal length experienced a decrease in alpha value as the height increased.

A fourth order response from the fitted curve shows clearly that the material does not follow a linear pattern for large deflection. The results of the Euler-Bernoulli equations show how poorly it can model large deflection. Additionally, the Euler-Bernoulli model does not account for the hyper-elasticity of the NinjaFlex®.

5 CONCLUSION

The expanding utilization of 3D printing has encouraged the invention of novel printing filaments, such as NinjaFlex®. This material proves to be highly useful because of its strength and ability to bend. However, a full knowledge of the behavior of this material under various loading conditions is still lacking. Previous work was limited to axial loading. The goal of this research to evaluate the behavior of cantilevered 3D printed NinjaFlex® specimens when subjected to loads inducing large deformation. A test matrix was produced with 27 different specimen configurations. Three specimens were printed for each of these configurations leading to a total of 81 specimens. A combination of digital camera and custom image processing techniques were used to monitor deflection of the tip point of the specimens under various loads. The results show that specimens representing the same configuration yielded fairly close results, indicating that the behavior of NinjaFlex® is repeatable. The results of a were compared to Euler-Bernoulli theorem. The large difference in the results confirms the need for a model that can account for the hyper-elasticity of the material and the large deflection specimens experience. Future work would be focused on developing such model.

REFERENCES

[1] Reppel, T. & Weinberg, K., Experimental determination of elastic and rupture properties of printed NinjaFlex. *Technische Mechanik*, **38**(1), 2018. DOI: 10.24352/UB.OVGU-2018-010.

[2] Messimer, P., O'Toole, B., & Trabia, M., Identification of the mechanical characteristics of 3D printed NinjaFlex®. *Proceeding of the ASME 2019 International Mechanical Engineering Congress and Exposition*. *vol. 9: Mechanics of Solids, Structures, and Fluids*, Salt Lake City, Utah, USA. 11–14 Nov. 2019. V009T11A004. ASME. DOI: 10.1115/IMECE2019-11674.

[3] Pitaru, et al., Investigating commercial filaments for 3D printing of stiff and elastic constructs with ligament-like mechanics. *Micromachines*, **11**, 2020. DOI: 10.3390/mi11090846.